HHS Public Access

Author manuscript

Nat Photonics. Author manuscript; available in PMC 2013 December 16.

Published in final edited form as:

Nat Photonics. 2013 March 1; 7(3): 205–209. doi:10.1038/nphoton.2012.336.

In vivo three-photon microscopy of subcortical structures within an intact mouse brain

Nicholas G. Horton[†,1], **Ke Wang**[†,1], **Demirhan Kobat**[†,1], **Catharine G. Clark**[2], **Frank W. Wise**[1], **Chris B. Schaffer**[2], and **Chris Xu**[*,1]

[1]School of Applied and Engineering Physics, Cornell University, Ithaca, New York 14853, USA

[2]Department of Biomedical Engineering, Cornell University, Ithaca, New York, 14853, USA

Abstract

Two-photon fluorescence microscopy (2PM)[1] enables scientists in various fields including neuroscience[2,3], embryology[4], and oncology[5] to visualize *in vivo* and *ex vivo* tissue morphology and physiology at a cellular level deep within scattering tissue. However, tissue scattering limits the maximum imaging depth of 2PM within the mouse brain to the cortical layer, and imaging subcortical structures currently requires the removal of overlying brain tissue[3] or the insertion of optical probes[6,7]. Here we demonstrate non-invasive, high resolution, *in vivo* imaging of subcortical structures within an intact mouse brain using three-photon fluorescence microscopy (3PM) at a spectral excitation window of 1,700 nm. Vascular structures as well as red fluorescent protein (RFP)-labeled neurons within the mouse hippocampus are imaged. The combination of the long excitation wavelength and the higher order nonlinear excitation overcomes the limitations of 2PM, enabling biological investigations to take place at greater depth within tissue.

Optical imaging plays a major role in both basic biological research and clinical diagnostics, providing a non-invasive or minimally-invasive microscopic imaging capability to investigate biological tissue. Optical image acquisition through significant depths of biological tissue, however, presents a major scientific challenge since tissue is extremely heterogeneous and the strong scattering of the various tissue components has historically restricted high-resolution optical imaging to thin sections or to superficial layers. The development of 2PM has significantly extended the penetration depth of high-resolution optical imaging, particularly for *in vivo* applications[8–12]. In the last 20 years, 2PM has enabled, in many fields for the first time, direct visualization of the normal behaviour of

Correspondence and requests for materials should be addressed to C. Xu (chris.xu@cornell.edu).

[†]These authors contributed equally to this work

[*]cx10@cornell.edu

Author Information Reprints and permissions information is available at www.nature.com/reprints.

The authors declare no competing financial interests.

Supplementary Information is linked to the online version of the paper at www.nature.com/naturephotonics.

Author Contributions C.X. initiated and supervised the study. N.G.H., K.W., D.K, and C.G.C. performed the experiments and data analysis. N.G.H., K.W., D.K., and C.X. contributed to the writing and editing of the manuscript. C.B.S. and C.X. contributed to the design of the experiments. F.W. and C.X. contributed to the laser source design.

cells in their natural environment as well as their responses to systematic manipulations[3,13]. Two-photon excitation of fluorescent molecules in tissue depends on the ability of sufficient excitation light to reach the focus of the objective unscattered (i.e., ballistic excitation photons). The fundamental limitation on imaging depth for high-resolution 2PM is the signal-to-background ratio (SBR) of the excitation in scattering biological tissue[10,12] (derivation of SBR for 2PM in Supplementary Information), which for 2PM is typically between 5 and 6 effective attenuation lengths (l_e) below the tissue surface. For example, for 2PM in the mouse neocortex at 775-nm excitation (l_e ~130 μm), this depth limit is ~700 μm. An effective strategy for increasing the maximum imaging depth is using longer excitation wavelengths to reduce the attenuation of excitation light by tissue[11,12,14,15]. The optimum spectral window for excitation is determined by the trade-off between tissue scattering and absorption (typically dominated by water absorption in the near-infrared spectral region). Figure 1a shows the water absorption length (l_a)[16] and the calculated scattering length (l_s) of mouse brain tissue[10,12]. The combined effect of absorption and scattering is represented by l_e [i.e., $l_e=(1/l_a+1/l_s)^{-1}$]. Figure 1a clearly indicates that the optimum wavelength window in terms of tissue penetration is near 1,700 nm when both tissue scattering and absorption are considered.

A longer excitation wavelength lone cannot overcome the depth limit imposed by the SBR of 2PM. 3PM was first demonstrated in the 1990s[17–19], mainly to extend the spectral range of the excitation source (e.g., access the transition band from 230 to 300 nm using a mode-locked Titanium:Sapphire laser). A significant advantage of 3PM that has been largely overlooked is that three-photon excitation (3PE) provides significant improvement in the overall excitation localization[17]. The fluorescence of 3PE falls off as $\sim 1/z^4$ (where z is the distance away from the focal plane), while the fluorescence of two-photon excitation (2PE) falls off as $\sim 1/z^2$. Therefore, 3PE dramatically reduces the out-of-focus background in regions far away from the focal plane, improving the SBR by orders of magnitude when compared to 2PE (see Supplementary Fig. S1). In addition, 3PE allows a wide variety of existing fluorescent dyes, fluorescent proteins, and calcium indicators to be excited at the 1,700-nm spectral window (equivalent to a one-photon excitation of ~560 nm), eliminating the practical difficulty caused by the lack of fluorescent indicators at the 1,700-nm spectral excitation window for 2PE as well as the lack of good potential fluorescence detectors for the near infrared wavelengths at which such dyes would likely emit.

The amount of 3PE can be significantly increased by using a low duty cycle, high pulse-energy excitation source[17], while still maintaining a low average power that does not cause tissue heating[11]. We developed a novel high pulse-energy source at 1,675 nm (Fig. 1c) using soliton self-frequency shift (SSFS)[20,21] in a photonic crystal (PC) rod[22] pumped by a turn-key, energetic fibre laser at 1,550 nm (see Methods for details). The large mode-field area of the PC rod enables the generation of high soliton pulse energy for 3PE. The measured output soliton energy of our source is 67 nJ at 1 MHz repetition rate, which is the highest soliton energy ever achieved through SSFS in a solid-core fibre. The measured soliton pulse width is 65 fs (Fig. 1b). SSFS not only shifts the wavelength to the desired 1,700 nm spectral window but also compresses the pulse width by a factor of 6, both essential for deep tissue 3PM.

We performed *in vivo* imaging of mouse brain vasculature to demonstrate the capability of deep tissue imaging at 1,675 nm using 3PE (see Methods and Supplementary Fig. S2). The vasculature was labelled by a retro-orbital injection of dextran-coupled Texas Red dye (Invitrogen). We acquired a 1,400 μm deep stack, taken with 4 μm depth increments. Figure 2a shows the 3D reconstruction of the data. By employing the energetic excitation source we developed at ∼ 1,700 nm, the average power required for 3PM at the surface of the brain in our experiments is ∼ 3 mW, which is comparable to conventional 2PM. For optical sections within the first 0.8 mm of imaging depth, the excitation powers were adjusted so that approximately the same signal level, and thus the same signal-to-noise ratio (SNR), could be achieved at a constant frame time of 8 seconds (512 × 512 pixels per frame). Our excitation source was used at full power (22 mW at the sample surface) at depths beyond 0.8 mm, while the integration time was increased 2.5 times (20 s/frame). The myelinated axons in the external capsule (EC, a.k.a. "white matter") produce a bright third harmonic generation (THG) signal[23–25] (Figs. 2a,b), which delineates the boundaries of the EC. Our images show that the EC begins approximately 840 μm below the surface of the brain. The EC is approximately 116 μm thick, and the CA1 region of the hippocampus (CA1) begins approximately 956 μm below the surface of the brain. We were able to obtain high-resolution, high-contrast images of the blood vessels up to approximately 1,300 μm deep. From this data set, it is possible to determine a characteristic attenuation length (CAL) for 1,675-nm imaging in mouse brain tissue *in vivo*. For 3PE, we define the CAL as the depth at which the average fluorescence signal of the brightest 0.1% of pixels attenuates by $1/e^3$. Figure 4a shows the detected fluorescence signal as a function of imaging depth, from which the CALs are determined to be 365 μm between 56 μm and 840 μm (i.e., the neocortex), 137 μm between 840 μm and 956 μm (i.e., the EC), and 310 μm between 956 μm and 1,148 μm (i.e., the CA1). In comparison, we had previously measured the CAL of the cortex to be 131 μm at 775 nm and 285 μm at 1,280 nm[11,12]. Furthermore, with 2PM at 1280 nm, we were unable to penetrate the EC using the same aged animals at the same sagittal and coronal imaging position as reported here[12].

We also performed quantitative SBR measurements at four depths between 1,000 and 1,135 μm (i.e., within the CA1). The SBRs range from 79 to 119; two examples are shown in Figs. 2c,d. The measured SBRs are lower than predicted by theory (shown in Supplementary Fig. S1) due to the limited SNR of the images (signal level vs. the electronic noise floor) at these depths. Nonetheless, these SBR values are more than one order of magnitude higher than previous 2PM results at 1,280 nm at similar depths but without the presence of the highly scattering EC[12].

We also imaged RFP-labelled neurons in a B6.Cg-Tg(Thy1-Brainbow1.0)HLich/J mouse[26] through a cranial window (see Methods). In particular, the labelled cells include pyramidal neurons in the neocortex and the *stratum pyramidale* (SP), a dense layer of pyramidal neurons within the hippocampus. We acquired a 1,220 μm stack, taken with 4 μm depth increments. Imaging conditions were similar to those used in Fig. 2, except that our source was used at full power (22 mW) at 0.7 mm, and starting from 0.74 mm, the integration time was increased 2 times (16 s/frame). Beyond 0.9 mm, the integration time was increased by another 1.25 times (20 s/frame). Figure 3a shows the 3D reconstructions of the data along

with selected optical sections of the SP region. Bright fluorescence images with appearance nearly identical to THG images are obtained in the EC, indicating expression of RFP in the axons in EC (Fig. 3c,d). Labelled neurons in the SP can be seen 1,060-1,120 μm below the surface of the brain (Fig. 3a,c). Visualization of this layer is clear evidence of direct imaging of the mouse hippocampus through an intact brain (see Fig. 3b and Supplementary Fig. S3)[27]. Figure 4b shows the detected fluorescence signal as a function of imaging depth. From the slope of the line, we measured the CAL to be 401 μm between 36 μm and 840 μm (i.e., the neocortex) and 229 μm between 840 μm and 976 μm (i.e., the EC). The relative increase in signal at 1.1 mm is due to the cells in the SP. The fluorescence value was uneven within the hippocampus due to the layered distribution of the pyramidal neurons, which made a CAL calculation difficult in this region.

We measured the lateral brightness distribution of small features within the RFP-labelled mouse brain (Fig. 5a,b), which provides the upper bound of the lateral resolution. For example, at 644 μm and 844 μm depths of the mouse brain, the full widths at half maximum (FWHM) of lateral brightness distributions are ∼0.9 μm. The axial FWHM are measured to be between 5.1 and 5.5 μm (average 5.3 μm) for 5 capillary blood vessels at depths between 817 and 948 μm below the surface of the brain (two examples are shown in Figs. 5c,d). Taking into account that the minimum diameter of mouse capillary is ∼ 3 μm[28], these values indicated that the axial resolution (FWHM) of our system is ∼ 4.4 μm at these depths.

3PM at the new spectral window of 1,700 nm is potentially a powerful new tool for *in vivo*, high-resolution, deep tissue imaging. By further improving the excitation source and microscope optics at 1,700 nm, we estimate that at least one order of magnitude improvement in frame rate can be achieved. In addition, by increasing the energy of the pump pulse and optimizing the PC rod, a wavelength tuneable source that covers the entire “low attenuation” spectral window from 1,650 to 1,850 nm can be obtained, which will further increase the number of accessible fluorophores and fluorescent proteins for 3PE in the 1,700-nm spectral window.

Methods

Fibre-based excitation source

The pump source for SSFS is a compact, turn-key, fibre-based femtosecond laser (FLCPA-01C, Calmar), delivering 360 fs and linearly-polarized pulses with a 1 MHz repetition rate at 1,550 nm. SSFS is performed in a commercially available, 36 cm long, polarization maintained (PM) PC rod (DC-200-70-PM-Yb-ROD, NKT Photonics) with an effective mode area (A_{eff}) of 2,300 μm^2 at 1,550 nm. After collimation, a 1,600 nm long pass filter (LPF, 1600ALP, Omega Optical) is used to filter out the residual pump. The soliton shifts to 1,675 nm at an input pulse energy of 500 nJ. The pulse width of the soliton is measured by performing second order autocorrelation. The measured soliton pulse width, assuming a sech^2 intensity profile, is 65 femtoseconds (fs) (Fig. 1b). Due to the dispersion of microscope optics, the pulse width broadened to 79 fs after the objective. Pulse broadening due to propagation through brain tissue is mainly due to dispersion of water, since brain tissue is over 75% water. Our calculation shows that, after 2-mm of water (i.e., the working distance of our water immersion objective lens), the 79 fs pulse (originally chirped from 65

fs) will be further broadened to ∼100 fs. The effective thickness of the water layer (i.e., the water immersion layer plus the thickness of the tissue) is essentially independent of the imaging depth, making the pulse width approximately constant over the entire imaging depth.

Imaging Setup

Imaging is performed with a multiphoton microscope[11,12] (Supplementary Fig. S2). We use heavy water (D_2O), which is safe and widely available, instead of regular water as the immersion liquid in order to minimize the absorption of the 1,675 nm excitation by the liquid between the objective and the sample surface. The immersion D_2O is sealed from the moisture in the air because D_2O is hygroscopic. We use a photomultiplier tube (PMT) with a GaAsP photocathode (H7422-40, quantum efficiency (QE) at 600 nm ∼36%, Hamamatsu Photonics) to detect the fluorescence from Texas Red or RFP tdimer2(12). The filters are a 593-nm long-pass filter (Semrock) and a 630 ± 46 nm band-pass filter (Chroma Technology), respectively, for Texas Red and RFP tdimer2(12). The THG signal (558 nm) is detected through a 558±10 nm band-pass filter (Semrock) by an ultra bialkali PMT (R7600-200, QE at 560 nm ∼10%, Hamamatsu Photonics). A movable objective microscope head (MOM, Sutter Instrument Company) translates the objective axially to change the imaging depth within the sample. The field of view (FOV) for each image is 123 μm × 123 μm. A computer running the ScanImage[29] module with MATLAB (Mathworks) software controls translation of the objective and the image acquisition. Current generated by the PMT is converted to voltage (0.1 V/μA) and low-pass filtered (20 KHz) by a transimpedance amplifier (C7319, Hamamatsu Photonics). Analogue-to-digital conversion is performed by a data acquisition card (NI PCI-6110, National Instruments) at a sampling rate up to 5 million samples per second. Due to the low repetition rate of the laser (1 MHz), the pixel clock is roughly 15 microseconds, resulting in oversampling by our data acquisition card. For depth measurement, the slightly larger index of refraction in brain tissue (1.35 to 1.4 for the cortex[30,31] and as high as 1.467 for the white matter[31]), relative to water (∼ 1.33), results in a slight underestimate (5–10%) of the actual imaging depth within the tissue because the imaging depths reported here are the raw axial movement of the objective. For image processing, a median filter with a 1 pixel radius was applied.

For *in vivo* axial resolution measurements, we drew a line across the capillary vessels in the fast scanning direction, and measured the maximum brightness along this line at each depth to get the axial brightness profile. This approach partially mitigates the motion artefacts caused by heartbeat and breathing, and avoids the dark pixels inside the capillary vessel caused by the non-labelled blood cells.

Animal Procedures

Animal procedures were reviewed and approved by the Cornell Institutional Animal Care and Use Committee. We used male FVB/N mice (23 g, 10 weeks old, Charles River) for Texas Red-labelled vasculature imaging, and B6.Cg-Tg(Thy1-Brainbow1.0)HLich/J mice (18 g, 6 weeks old, The Jackson Laboratory) for RFP-labelled neuron imaging. Animals were prepared using the methods described by Kobat;[12] the craniotomies were performed centred at 2 mm posterior and 2 mm lateral to the Bregma point. Prior to imaging the FVB/n

mice, 200 μl of 70 kDa Texas Red-Dextran (Invitrogen, dissolved at 5% w/v in saline) was retro-orbitally injected to label the vasculature. The B6.Cg-Tg(Thy1-Brainbow1.0)HLich/J mice were not subjected to Cre recombinase, thus the only fluorescent protein expression was from RFP tdimer2(12).

Perfusion and slicing

Mice (B6.Cg-Tg(Thy1-Brainbow1.0)HLich/J) were euthanized and perfused. Brain slices were prepared and imaged using the post-mortem histology methods described by Rosidi.[32]

Supplementary Material

Refer to Web version on PubMed Central for supplementary material.

Acknowledgments

This work is partially funded by grants from the National Institutes of Health (NIH) (R01CA133148), (R01EB014873), and (R21RR032392). N.G.H. is supported by the National Science Foundation, Graduate Research Fellowship Program (DGE-0707428). We acknowledge discussions with D. Dombeck, as well as N. Nishimura and J. Rubin for preparation of the *ex vivo* brain slices.

References

1. Denk W, Strickler JH, Webb WW. Two-photon laser scanning fluorescence microscopy. Science. 1990; 248:73–76. [PubMed: 2321027]
2. Kerr JND, Denk W. Imaging in vivo: watching the brain in action. Nat Rev Neurosci. 2008; 9:195–205. [PubMed: 18270513]
3. Dombeck DA, Harvey CD, Tian L, Looger LL, Tank DW. Functional imaging of hippocampal place cells at cellular resolution during virtual navigation. Nat Neurosci. 2010; 13:1433–1440. [PubMed: 20890294]
4. Olivier N, et al. Cell lineage reconstruction of early zebrafish embryos using label-free nonlinear microscopy. Science. 2010; 329:967–971. [PubMed: 20724640]
5. Williams RM, et al. Strategies for high-resolution imaging of epithelial ovarian cancer by laparascopic nonlinear microscopy. Transl Oncol. 2010; 3:181–194. [PubMed: 20563260]
6. Jung JC, Mehta AD, Aksay E, Stepnoski R, Schnitzer MJ. In vivo mammalian brain imaging using one- and two-photon fluorescence microendoscopy. J Neurophysiol. 2004; 92:3121–3133. [PubMed: 15128753]
7. Levene MJ, Dombeck DA, Kasischke KA, Molloy RP, Webb WW. In vivo multiphoton microscopy of deep brain tissue. J Neurophysiol. 2004; 91:1908–1912. [PubMed: 14668300]
8. Kleinfeld D, Mitra PP, Helmchen F, Denk W. Fluctuations and stimulus induced changes in blood flow observed in individual capillaries in layers 2 through 4 of rat neocortex. Proc Natl Acad Sci U S A. 1998; 95:15741–15746. [PubMed: 9861040]
9. Svoboda K, Helmchen F, Denk W, Tank DW. Spread of dendritic excitation in layer 2/3 pyramidal neurons in rat barrel cortex in vivo. Nat Neurosci. 1999; 2:65–73. [PubMed: 10195182]
10. Theer P, Hasan MT, Denk W. Two-photon imaging to a depth of 1000 μm in living brains by use of a Ti:Al_2O_3 regenerative amplifier. Opt Lett. 2003; 28:1022–1024. [PubMed: 12836766]
11. Kobat D, et al. Deep tissue multiphoton microscopy using longer wavelength excitation. Opt Express. 2009; 17:13354–13364. [PubMed: 19654740]
12. Kobat D, Horton NG, Xu C. In vivo two-photon microscopy to 1.6-mm depth in mouse cortex. J Biomed Opt. 2011; 16:106014. [PubMed: 22029361]
13. Helmchen F, Denk W. Deep tissue two-photon microscopy. Nat Methods. 2005; 2:932–940. [PubMed: 16299478]

14. Balu M, et al. Effect of excitation wavelength on penetration depth in nonlinear optical microscopy of turbid media. J Biomed Opt. 2009; 14:010508. [PubMed: 19256688]
15. Sacks ZS, Kurtz R, Juhasz T, Spooner G, Mouroua GA. Subsurface Photodisruption in Human Sclera: Wavelength Dependence. Ophthalmic Surg Lasers Imaging. 2003; 34:104–113. [PubMed: 12665225]
16. Kou L, Labrie D, Chylek P. Refractive indices of water and ice in the 0.65- to 2.5-μm spectral range. Appl Opt. 1993; 32:3531–3540. [PubMed: 20829977]
17. Xu C, Zipfel W, Shear JB, Williams RM, Webb WW. Multiphoton fluorescence excitation: new spectral windows for biological nonlinear microscopy. Proc Natl Acad Sci U S A. 1996; 93:10763–10768. [PubMed: 8855254]
18. Hell SW, et al. Three-photon excitation in fluorescence microscopy. J Biomed Opt. 1996; 1:71–74. [PubMed: 23014645]
19. Wokosin DL, Centonze VE, Crittenden S, White J. Three-photon excitation fluorescence imaging of biological specimens using an all-solid-state laser. Bioimaging. 1996; 4:208–214.
20. Zysset B, Beaud P, Hodel W. Generation of optical solitons in the wavelength region 1.37–1.49 μm. Appl Phys Lett. 1987; 50:1027–1029.
21. Wang K, Xu C. Tunable high-energy soliton pulse generation from a large-mode- area fiber and its application to third harmonic generation microscopy. Appl Phys Lett. 2011; 99:071112.
22. Limpert J, et al. High-power rod-type photonic crystal fiber laser. Opt Express. 2005; 13:1055–1058. [PubMed: 19494970]
23. Barad Y, Eisenberg H, Horowitz M, Silberberg Y. Nonlinear scanning laser microscopy by third harmonic generation. Appl Phys Lett. 1997; 70:922–924.
24. Müller M, Squier J, Wilson KR, Brakenhoff GJ. 3D microscopy of transparent objects using third-harmonic generation. J Microsc. 1998; 191:266–274. [PubMed: 9767491]
25. Farrar MJ, Wise FW, Fetcho JR, Schaffer CB. In vivo imaging of myelin in the vertebrate central nervous system using third harmonic generation microscopy. Biophys J. 2011; 100:1362–1371. [PubMed: 21354410]
26. Livet J, et al. Transgenic strategies for combinatorial expression of fluorescent proteins in the nervous system. Nature. 2007; 450:56–62. [PubMed: 17972876]
27. Franklin, KBJ.; Paxinos, G. Mouse brain in stereotaxic coordinates. Academic Press; London: 2008.
28. Murphy PA, et al. Notch4 normalization reduces blood vessel size in arteriovenous malformations. Sci Transl Med. 2012; 4:117ra8.
29. Pologruto TA, Sabatini BL, Svoboda K. ScanImage: flexible software for operating laser scanning microscopes. Biomed Eng Online. 2003; 2:13. [PubMed: 12801419]
30. Binding J, et al. Brain refractive index measured in vivo with high-NA defocus corrected full-field OCT and consequences for two-photon microscopy. Opt Express. 2011; 19:4833–4847. [PubMed: 21445119]
31. Bacallao, R.; Sohrab, S.; Phillips, C. Guiding Principles of Specimen Preservation for Confocal Fluorescence Microscopy. In: Pawley, JB., editor. Handbook Of Biological Confocal Microscopy. p. 368-380.
32. Rosidi NL, et al. Cortical microhemorrhages cause local inflammation but do not trigger widespread dendrite degeneration. Plos One. 2011; 6:e26612. [PubMed: 22028924]

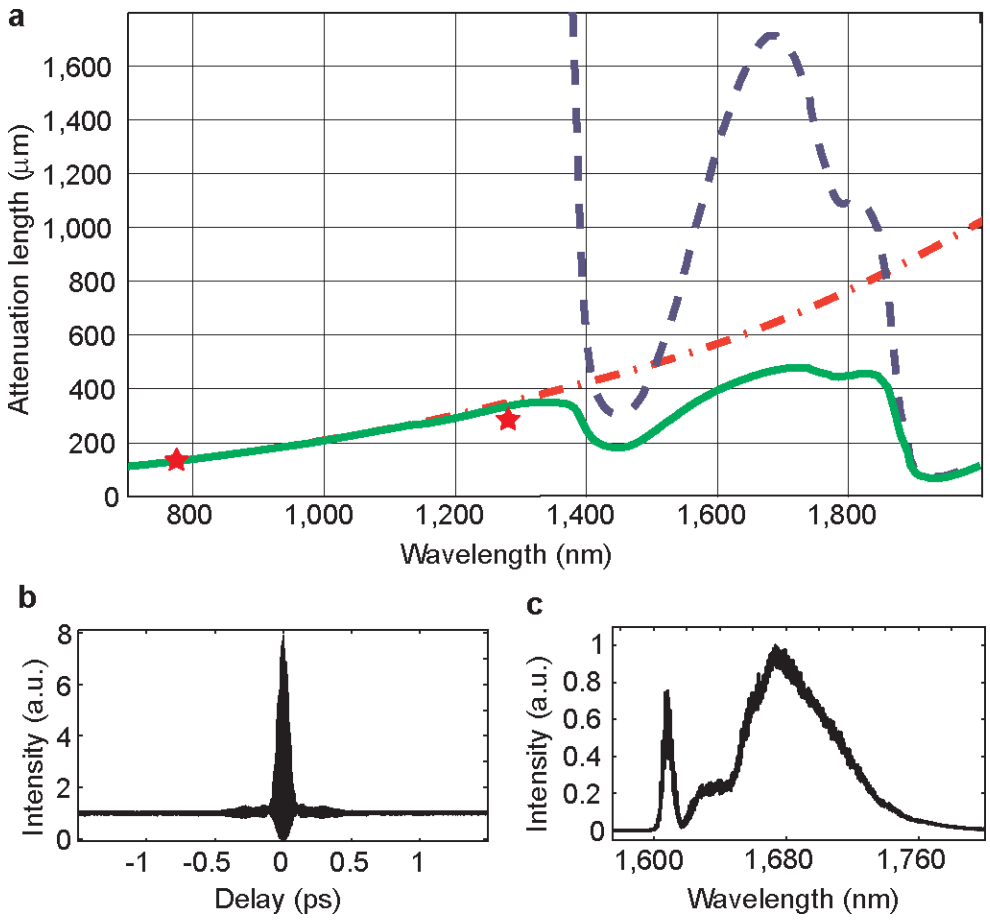

Figure 1. Wavelength-dependent attenuation length in brain tissue and measured laser characteristics

a, Attenuation spectrum of a tissue model based on Mie scattering and water absorption, showing the absorption length of water (blue dash line), the scattering length of mouse brain cortex (red dash-dot line), and the combined effective attenuation length (green solid line). The scattering length is calculated using Mie theory for a tissue-like phantom solution containing 1 μm diameter polystyrene beads at a concentration of 5.4×10^{9}/ml, which resembles the scattering property of the cortex (i.e., grey matter). The red stars indicate the reported attenuation lengths for mouse cortex *in vivo* from previous work[11]. **b**, **c**, The measured second-order interferometric autocorrelation trace (**b**) and the corresponding spectrum (**c**) of the 1,675-nm soliton generated in the PC rod. The soliton energy, integrated from 1,617 nm, is 67 nJ.

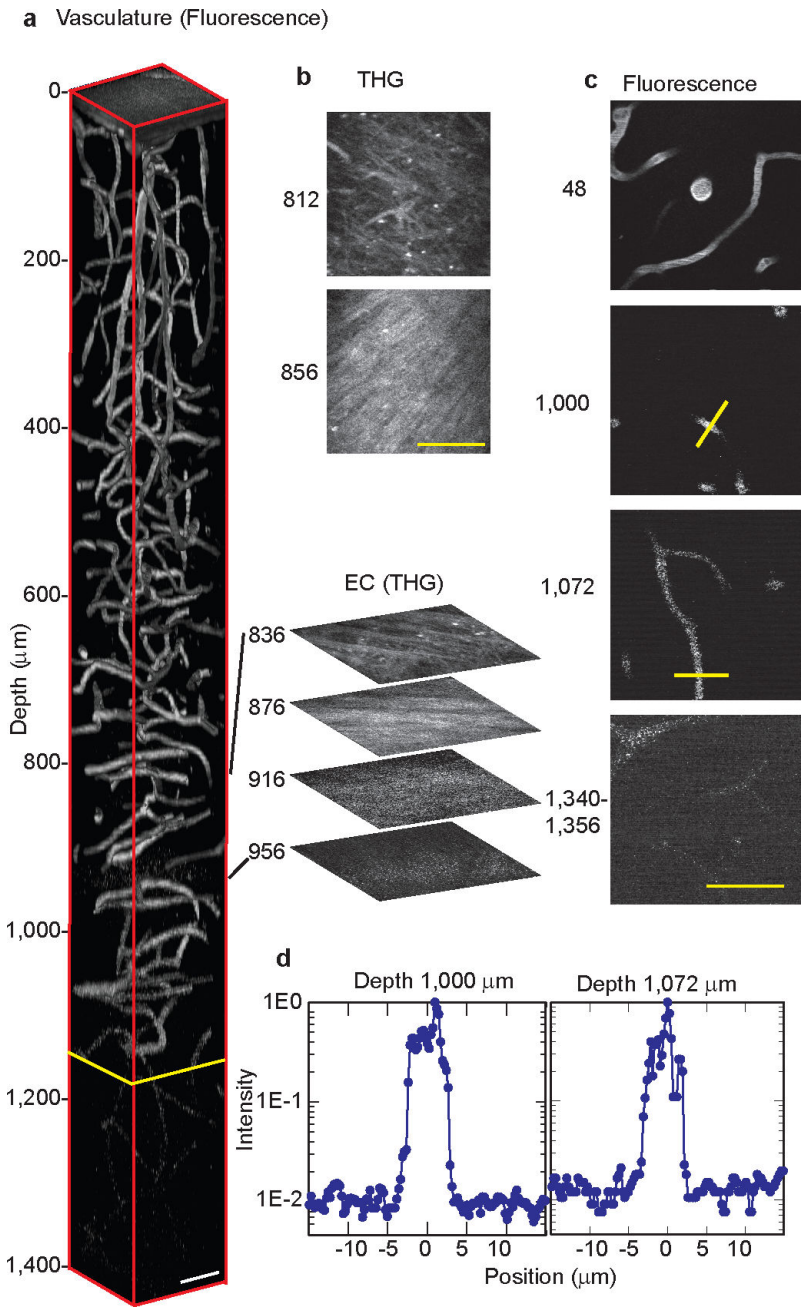

Figure 2. ***In vivo*** **3PM images of Texas-red-dextran labeled mouse brain vasculature**

a, 3D reconstruction of 3PM images of the brain of an FVB/N mouse. The EC extends from approximately 840 to 956 μm below the surface of the brain. Frames deeper than 1,136 μm (yellow line) were normalized to the frame at 1,136 μm; all other frames were individually normalized. The expanded optical sections to the right are representative THG images from the EC region of the brain. **b**, **c, d**, Normalized x-y frames of the THG **(b)** and fluorescence signal **(c)** at various depths. The bottom frame in **(c)** is a z projection of 20 μm. The fluorescence profiles of the lines across the vessels in **(c)** are displayed in semi-logarithmic

plots **(d)**, which are used for the SBR calculation. Background is calculated by averaging the intensity values between −15 and −5 μm and between 5 and 15 μm. All scale bars are 50 μm.

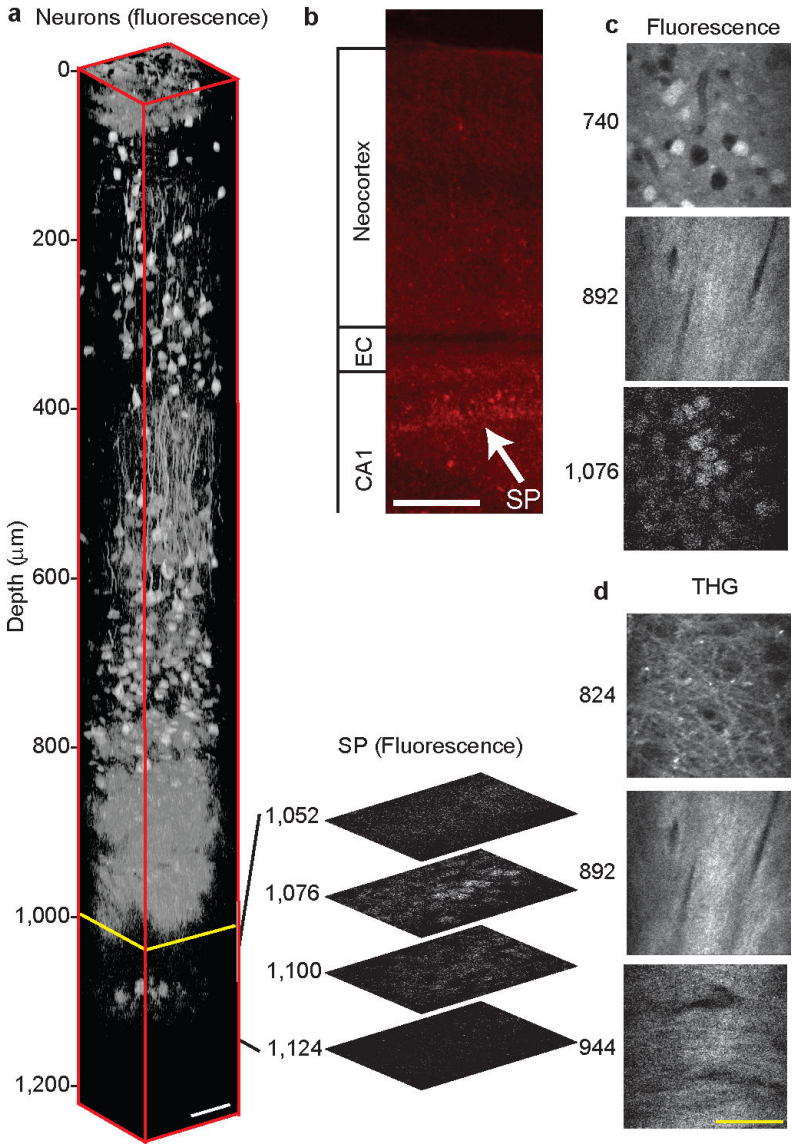

Figure 3. ***In vivo*** **3PM images of RFP-labeled neurons in mouse brain**

a, 3D reconstruction of 3PM images in the brain of a B6.Cg-Tg(Thy1-Brainbow1.0)HLich/J mouse, which contains RFP-labelled pyramidal neurons. Frames deeper than 992 μm (yellow line) were normalized to the frame at 1,076 μm (i.e., the SP); all other frames were individually normalized. The expanded optical sections to the right are representative fluorescence images of the SP. The EC extends from approximately 840 to 976 μm below the surface of the brain, and the SP extends from approximately 1,060 to 1,120 μm below the surface. The scale bar is 50 μm. **b**, Epifluorescence image of the coronal section of the mouse brain at approximately the same location to that shown in **(a)**. The white arrow indicates the SP. The scale bar is 250 μm. **c**, **d**, Normalized x-y frames of the fluorescence (**c**) and THG (**d**) signal at various depths. The scale bar is 50 μm.

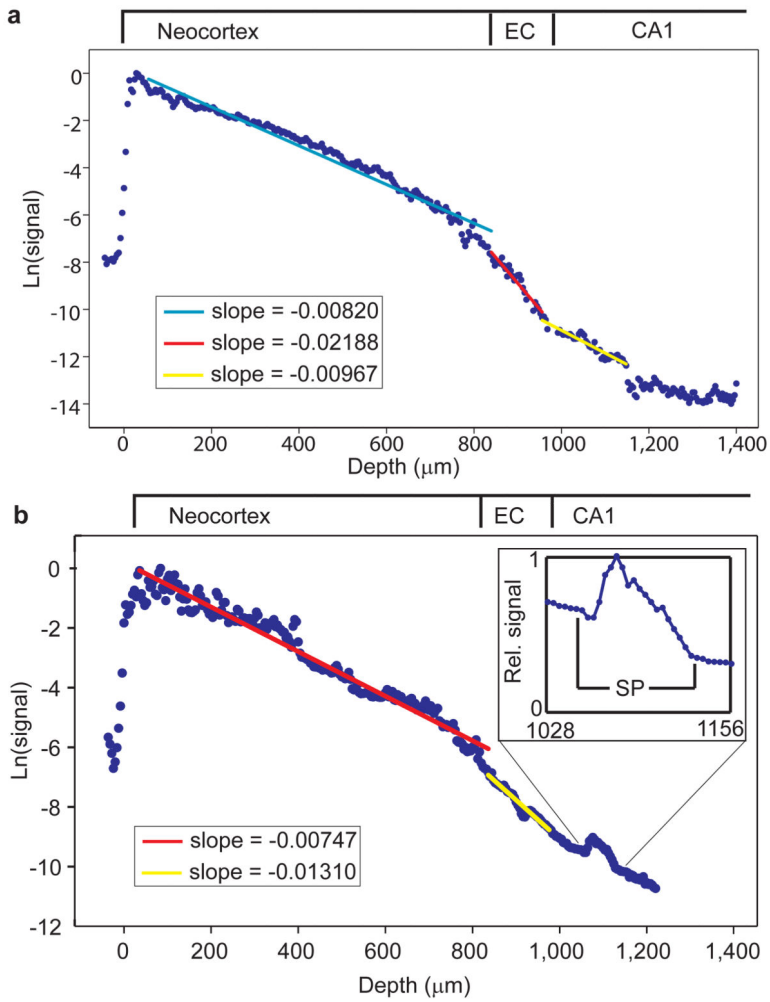

Figure 4. Fluorescence signal attenuation curves of *in vivo* experiments

a, **b,** Semi-logarithmic plots of the fluorescence signal of the images in Fig. 2a (**a**) and Fig. 3a (**b**), normalized to the cubic of the laser power versus depth.

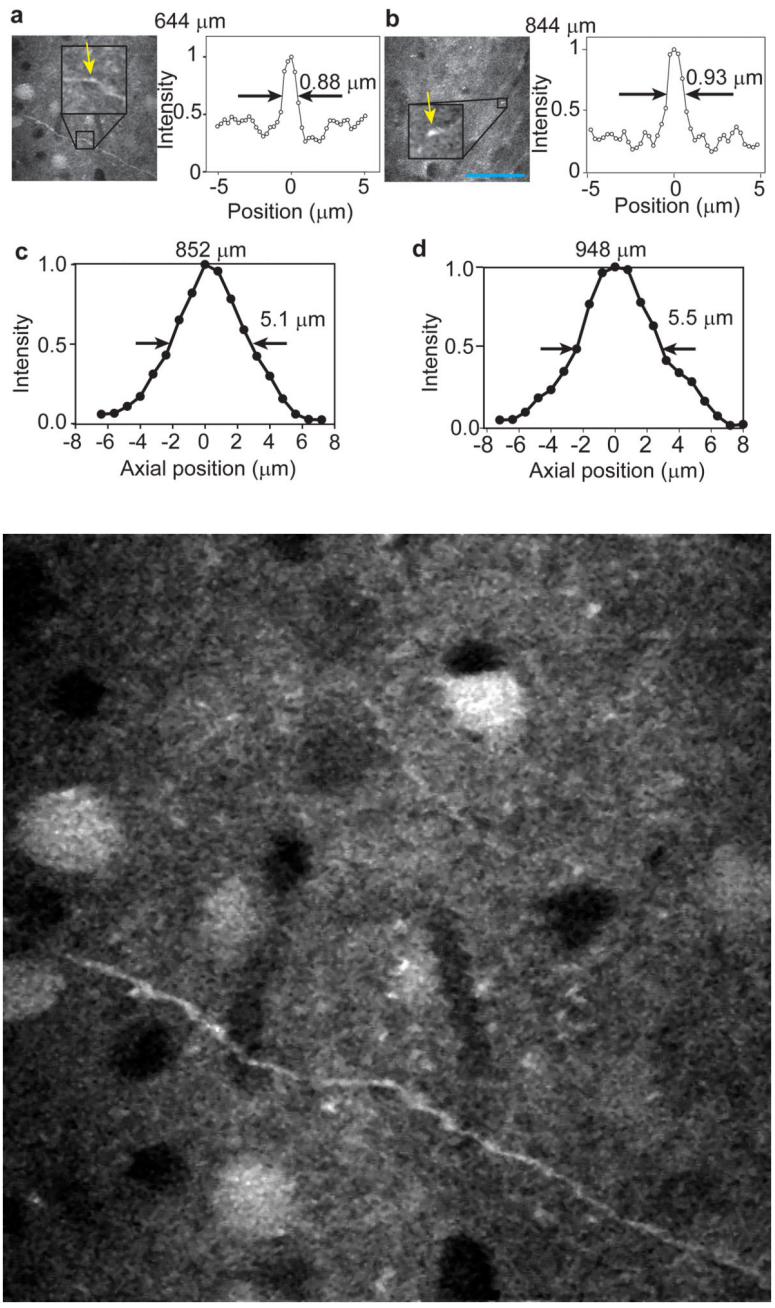

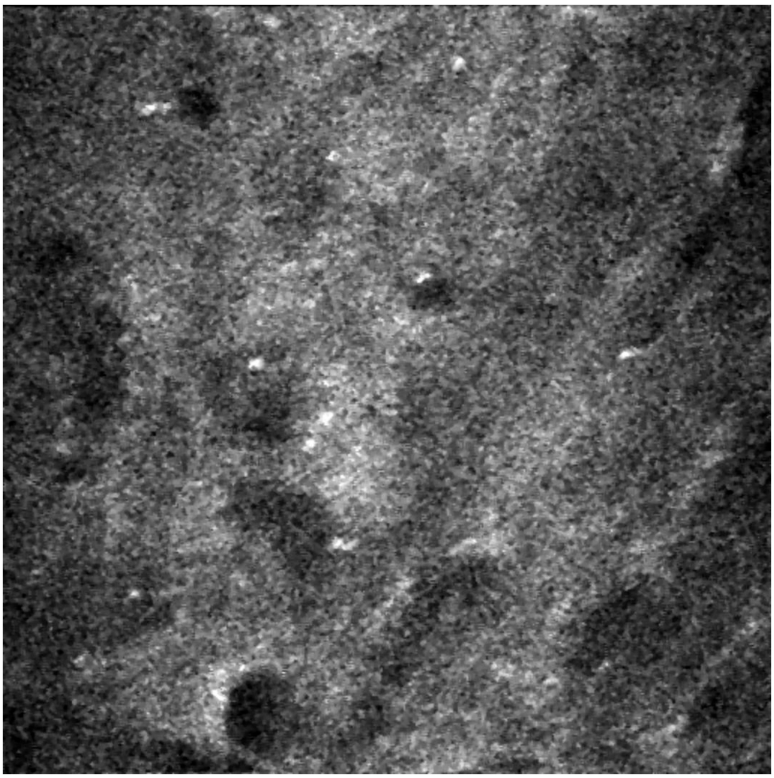

Figure 5. Resolution characterization of the 3PM

Intensity line profiles are used to characterize the lateral resolution. **a**, **b**, Sample x-y frames at 644 μm (**a**) and 844μm depth (**b**) of the B6.Cg-Tg(Thy1-Brainbow1.0)HLich/J mouse, where a line profile on the right is taken across a labelled neural process (indicated by yellow arrows). The scale bar is 50 μm. **c, d**, Axial measurements of FVB/n mouse Texas-red stained capillary vessels at 852 μm (c) and 948 μm (d) depth.